Improving quantum gate fidelities using optimized Euler angles

K. Ch. Chatzisavvas,[1,*] G. Chadzitaskos,[2,†] C. Daskaloyannis,[3,‡] and S. G. Schirmer[4,5,§]
[1]*Department of Theoretical Physics, Aristotle University of Thessaloniki, 54124 Thessaloniki, Greece*
[2]*Department of Physics, FNSPE, Czech Technical University, Brehova 7, CZ-115 19 Praha 1, Czech Republic*
[3]*Mathematics Department, Aristotle University of Thessaloniki, 54124 Thessaloniki, Greece*
[4]*Department of Applied Maths and Theoretical Physics, University of Cambridge, Wilberforce Road, Cambridge CB3 0WA, United Kingdom*
[5]*Department of Maths and Statistics, University of Kuopio, P.O. Box 1627, 70211 Kuopio, Finland*
(Received 9 July 2009; published 23 November 2009)

An explicit algorithm for calculating the optimized Euler angles for both qubit state transfer and gate engineering given two *arbitrary* fixed Hamiltonians is presented. It is shown how the algorithm enables us to efficiently implement single qubit gates even if the control is severely restricted and the experimentally accessible Hamiltonians are far from orthogonal. It is further shown that using the optimized Euler angles can significantly improve the fidelity of quantum operations even for systems where the experimentally accessible Hamiltonians are nearly orthogonal. Unlike schemes such as composite pulses, the proposed scheme does not significantly increase the number of local operations or gate operation times.

DOI: 10.1103/PhysRevA.80.052329 PACS number(s): 03.67.Lx, 02.30.Yy, 07.05.Dz

I. INTRODUCTION

Quantum computing [1] generally relies on the decomposition of arbitrary multiqubit operations into products of elementary single and two-qubit gates, which must be implemented with very high fidelity. Although the availability of an entangling two-qubit gate is crucial for universal quantum computing [2], single qubit operations dominate virtually any decomposition of a multiqubit quantum gate. For example, if we decompose a two-qubit gate into two-qubit gates that can be generated by a natural Ising interaction and local operations using the Cartan decomposition [3], at most three two-qubit terms are required in addition to 12 single qubit rotations. Therefore the fidelity of single qubit gates is critical, as even small single qubit gate errors quickly accumulate, resulting in poor multiqubit gate fidelities even if the entangling gate is perfect.

One approach to improving gate fidelities and gate operation times is using optimal control. In general, optimal control fields can be derived by simultaneous optimization of many control parameters using numerical algorithms based on Poyntriagin's Maximum principle (see, e.g., [4–9]). Optimal control may be the only viable option for implementing quantum gates for systems with highly complex Hamiltonians including off-resonant excitation and multibody fixed coupling terms [10], but numerical optimization can be time consuming and the resulting optimal control fields can be quite complicated and not necessarily easy to implement. By contrast, geometric control, vaguely inspired by nuclear magnetic resonance (NMR) [11], requires only sequences of simple pulses to implement arbitrary single and multiqubit gates. Although compared optimally designed pulses the results may be suboptimal, this approach remains popular especially in an experimental setting, due to its conceptual and experimental simplicity. However, there are limits to the applicability of standard techniques such as the Euler and Cartan decomposition, for instance, when we cannot implement local rotations about orthogonal axes, a situation that arises in various settings, from global electron-spin architectures [12] to charge-based semiconductor quantum dot systems [13].

Geometric control generally relies heavily on Lie group decompositions such as the standard Euler decomposition [14] of rotations in $\mathbb{R}^3$, which provides an explicit formula for decomposing any rotation in $\mathbb{R}^3$ into a sequence of (at most) three rotations about two fixed, orthogonal axes, $\hat{\mathbf{g}}$ and $\hat{\mathbf{h}}$. Due to the equivalence of SU(2) and SO(3) [$\mathrm{SO}(3) \simeq \mathrm{SU}(2)/(-1,1)$], it also provides an explicit scheme to decompose any special unitary operator in SU(2) into elementary complex rotations, combined with the generalized Cartan decomposition for multiqubit gates, it provides a basis for generating arbitrary multiqubit gates. The main drawback of the standard Euler angle decomposition is that requires orthogonal rotation axes, or respectively, Hamiltonians, while the Hamiltonians that are experimentally easily accessible are often at best approximately orthogonal, subject to certain simplifications such as negligible drift, rotating wave approximation, etc. Applying the standard Euler angle decomposition when the available basic Hamiltonians are not orthogonal reduces the fidelity of most local gates, and hence virtually all multiqubit quantum gates, regardless of the quality of the entangling gates, decoherence or other sources of noise that may reduce the fidelities of quantum operations. This is a significant problem for applications such as quantum computation, where extremely high accuracy of the elementary gates is a prerequisite for scalability.

One way to improve the accuracy of elementary gates is using composite pulse sequences [15–17] to compensate for certain systematic errors such as rotation axis alignment and rotation angle errors. Such approaches have proved to be

*kchatz@auth.gr
†goce.chadzitaskos@fjfi.cvut.cz
‡daskalo@math.auth.gr
§sgs29@cam.ac.uk

extremely valuable in ensemble-based quantum computing schemes such as liquid-state NMR, where multiple qubits are encoded into different nuclear spins of a larger molecule, and the system consists of an ensemble of a large number of identical molecules in solution. Due to magnetic field gradients, diffusion processes, and intermolecular interactions, the actual fields experienced by the individual molecules are subject to fluctuations, resulting in rotation angle errors, and to a lesser extent, rotation axis errors. Composite pulses reduce these errors by replacing simple unitary operations (rotations) with sequences of rotations designed to "cancel" certain errors. However, this systematic error cancellation comes at the expense of increased overhead in the number of elementary operations, and hence time required to implement a single quantum gate, especially if the systematic errors are so large as to require the use of concatenated composite pulses [18]. This can exacerbate other problems such as decoherence. Composite pulses can be applied to implement gates that are robust with respect to model uncertainty in nonensemble-based systems. However, unlike in ensemble-based schemes, where the systematic errors are a direct consequence of the fact that different molecules in the ensemble experience different forces, systematic errors due to model uncertainty in nonensemble systems can be minimized by experimental system identification [19–22], and this has been shown to be advantageous in that it reduces to level of concatenation required for composite pulse sequences [18]. In this paper we show that if the actual Hamiltonians are known to sufficient accuracy then we can significantly improve gate fidelities with minimal overhead simply by optimizing the Euler angles in the decomposition, potentially completely eliminating the need for expensive composite pulse sequences.

II. QUANTUM GATE ENGINEERING USING LIE GROUP DECOMPOSITIONS

Quantum computing generally relies on decomposing multiqubit gates into products of elementary single and two-qubit gates, which can be applied simultaneously or sequentially to produce a desired unitary evolution. Following the idea of using realistic physical Hamiltonians to generate quantum gates efficiently [23–25], one approach is to decompose a desired unitary operation U into elementary unitary operations that can be easily generated by natural Hamiltonian flows of the system. For instance, given a system with a natural Ising coupling $\sigma_z^{(1)}\sigma_z^{(2)}$ between adjacent qubits, and the ability to generate arbitrary local unitary operations, any two-qubit gate can be factorized into a product of local operations, and the natural flows $Z(t)=\exp(-it\sigma_z^{(1)}\sigma_z^{(2)})$ using the Cartan decomposition [26]

$$U = U_1[K_x^\dagger Z(\alpha_1)K_x][K_y^\dagger Z(\alpha_2)K_y]Z(\alpha_3)U_2, \tag{1}$$

where $Z(\alpha)$ corresponds to free evolution of the system under the Ising-coupling Hamiltonian for the time $t=\alpha$, and U_1, U_2, K_x, and K_y are simultaneous local operations on both qubits. U_1 and U_2 depend on the particular gate to be implemented, while $K_x=U_x^{(1)}(\pi)\otimes U_x^{(2)}(\pi)$, where $U_x^{(k)}(\alpha)=\exp(-i\frac{\alpha}{2}\sigma_x^{(k)})$, $k=1,2$, and similarly for K_y. The Cartan decomposition can be generalized to interactions involving more than two qubits [7], and an explicit algorithm to calculate the generalized Cartan decomposition was presented in [27]. Similar decompositions also exist for other natural nonlocal Hamiltonians but we still require very accurate single qubit gates. In principle such gates are easy to implement. Any $W\in \mathrm{SU}(2)$ can be written as

$$W(\alpha,\beta,\gamma) = \begin{pmatrix} \cos(\alpha)e^{i\beta} & \sin(\alpha)e^{i\gamma} \\ -\sin(\alpha)e^{-i\gamma} & \cos(\alpha)e^{-i\beta} \end{pmatrix} \tag{2}$$

where $0\le\alpha\le\frac{\pi}{2}$, $0\le\beta,\gamma<2\pi$. We also have $W=\exp(-i\tilde{H})$ with $-i\tilde{H}\in \mathrm{su}(2)$, i.e.,

$$\tilde{H} = \tilde{H}(\mathbf{d}) = d_x\sigma_x + d_y\sigma_y + d_z\sigma_z \tag{3}$$

with the usual Pauli matrices

$$\sigma_x = \begin{pmatrix} 0 & 1 \\ 1 & 0 \end{pmatrix}, \quad \sigma_y = \begin{pmatrix} 0 & -i \\ i & 0 \end{pmatrix}, \quad \sigma_z = \begin{pmatrix} 1 & 0 \\ 0 & -1 \end{pmatrix}. \tag{4}$$

Let $\mathbf{d}=(d_x,d_y,d_z)$ with $\Omega=\|\mathbf{d}\|$ and $\mathbf{n}=\Omega^{-1}\mathbf{d}$. As $H^2=\Omega^2\mathbf{I}$, where $\mathbf{I}$ is the identity matrix, we have

$$\begin{aligned} e^{-itH} &= \exp[-i\Omega t(n_x\sigma_x + n_y\sigma_y + n_z\sigma_z)] \\ &= \cos(\Omega t)\mathbf{I} - i\sin(\Omega t)(n_x\sigma_x + n_y\sigma_y + n_z\sigma_z) \\ &= \begin{pmatrix} \cos(\Omega t) - in_z\sin(\Omega t) & -(n_y + in_x)\sin(\Omega t) \\ (n_y - in_x)\sin(\Omega t) & \cos(\Omega t) + in_z\sin(\Omega t) \end{pmatrix} \end{aligned}$$

and comparison of the last equation with Eq. (2) shows that $W=\exp(-iTH)$ if we choose $\mathbf{n}$, Ω and T such that

$$\Omega T = \arccos(\cos\alpha\cos\beta) \tag{5a}$$

$$\mathbf{n} = -S^{-1}(\sin\alpha\sin\gamma, \sin\alpha\cos\gamma, \cos\alpha\sin\beta) \tag{5b}$$

with $S=\sin(\Omega T)$. Thus, if we have full control over the single qubit Hamiltonians then we can implement any single qubit gate in a single step, and if there are no constraints on the magnitude Ω of the Hamiltonian then the gate operation time T can be made arbitrarily small.

Unfortunately, for most physical systems we cannot implement arbitrary Hamiltonians even locally. For example, the single qubit Hamiltonians for many potential qubit systems from ions to quantum dots are of the form $H=\frac{1}{2}(d_z\sigma_z + d_x\sigma_x)$ or $H=\frac{1}{2}(d_x\sigma_x+d_y\sigma_y)$, restricting us to rotations about axes in the xz or xy planes, respectively. If we have sufficient control over both d_x and d_z such as to be able to perform rotations about two orthogonal axes in the plane, then we can still implement arbitrary single qubit gates using the standard Euler decomposition, e.g.,

$$W(\alpha,\beta,\gamma) = U_z\left(\beta+\gamma-\frac{\pi}{2}\right)U_x(\alpha)U_z\left(\beta-\gamma+\frac{\pi}{2}\right), \tag{6}$$

where $U_x(\alpha)=\exp(i\frac{\alpha}{2}\sigma_x)$ and $U_z(\alpha)=\exp(i\frac{\alpha}{2}\sigma_z)$ are elementary rotations about the x and z axis, respectively.

However, in practice there are often more constraints, limiting us to varying one or both parameters within a certain range. For example, for certain solid-state architectures such as charge-based semiconductor quantum dot systems [13], it

is difficult or impossible to dynamically control the tunnel coupling d in the model Hamiltonian $H=\Delta\omega\sigma_z+d\sigma_x$. Thus $d\in[d_{\min},d_{\max}]$ and if $d_{\min}>0$ then we cannot implement rotations about the z axis, no matter how much control we have over the energy level splitting $\Delta\omega$, and practical constraints often make it impossible to find operating parameters $(\Delta\omega_1,d_1)$ and $(\Delta\omega_2,d_2)$ such that the corresponding Hamiltonians are exactly orthogonal. The same problem arises for other architectures where the amount of control is limited, such as global electron-spin systems where many electron spins in quantum dots are simultaneously controlled by a fixed global field, and we can only control the detuning $\Delta\omega$ of individual spins from the global field via local voltage gates [12]. In other cases $\Delta\omega$ may be fixed while we have limited control over the coupling strength d_x or Rabi frequency.

In these examples (and other similar systems) we have a fixed drift Hamiltonian and constraints on a controllable parameter. Without loss of generality, let us consider $H(\kappa)=\frac{d}{2}(\sigma_x+\kappa\sigma_z)$ with $d>0$ fixed and $\kappa\in[0,\kappa_{\max}]$. $\mathrm{Tr}(\sigma_x\sigma_z)=0$ and $\mathrm{Tr}(\sigma_x^2)=\mathrm{Tr}(\sigma_z^2)=\mathrm{Tr}(\mathbf{I})=2$ shows that the Hilbert-Schmidt inner product $\langle H(\kappa_1)|H(\kappa_2)\rangle=\mathrm{Tr}[H(\kappa_1)^\dagger H(\kappa_2)]$ satisfies

$$\langle H(\kappa_1)|H(\kappa_2)\rangle\le\langle H(0)|H(\kappa_{\max})\rangle=\frac{d^2}{2},\tag{7}$$

and $\|H(\kappa)\|=\sqrt{\langle H(\kappa)|H(\kappa)\rangle}=d\sqrt{(1+\kappa^2)/2}$. Thus, provided $d\neq0$, the angle ζ between the Hamiltonians $H(0)$ and $H(\kappa_{\max})$ is determined by

$$\cos\zeta=\frac{\langle H(0)|H_{\kappa_{\max}}\rangle}{\|H(0)\|\|H_{\kappa_{\max}}\|}=\frac{1}{\sqrt{1+\kappa_{\max}^2}}.\tag{8}$$

Thus, $\zeta\to\frac{\pi}{2}$ only for $\kappa_{\max}\to\infty$. For any finite value of $\kappa_{\max}$ the maximum angle between the accessible rotation axes will be less than $\frac{\pi}{2}$. If we use the standard Euler decomposition of a single qubit gate

$$U=U_x(\alpha)U_z(\beta)U_x(\gamma),\tag{9}$$

assuming $U_x(\alpha)=\exp(-i\frac{\alpha}{2}X)$ and $U_z(\beta)=\exp(-i\frac{\beta}{2}Z)$, but the actual "$z$" rotation is a rotation about $\tilde{Z}=X\cos\zeta+Z\sin\zeta$ with $\zeta=(1\pm\epsilon)\frac{\pi}{2}$ then the gate actually implemented is

$$\tilde{U}=U_x(\alpha)U_z^\epsilon(\beta)U_x(\gamma)\tag{10}$$

with $U_z^\epsilon(\beta)=\exp(-i\frac{\beta}{2}\tilde{Z})$. If there are no other errors the gate fidelity will be

$$\begin{aligned}\mathcal{F}(\beta,\epsilon)&=\frac{1}{2}|\mathrm{Tr}(U^\dagger\tilde{U})|=\frac{1}{2}|\mathrm{Tr}[U_z(\beta)^\dagger U_z^\epsilon(\beta)]|\\&=\cos^2(\beta/2)[1-\cos(\epsilon\pi/2)]+|\cos(\epsilon\pi/2)|\end{aligned}\tag{11}$$

and the gate error $\mathcal{E}(\beta,\epsilon)=1-\mathcal{F}(\beta,\epsilon)$. Thus the maximum single qubit gate error is $1-|\cos(\epsilon\frac{\pi}{2})|=\mathcal{E}(\pm\pi,\epsilon)$ and, noting $\langle\cos^2(x)\rangle=\frac{1}{2}$, the average single qubit gate error is $\mathcal{E}_{\mathrm{avg}}(\epsilon)=\frac{1}{2}[1-\cos(\epsilon\frac{\pi}{2})]$, and for the maximum single qubit error to be below 10^{-4}, the rotation angle error must be less than $\epsilon=0.9\%$ or equivalently

$$\cos\left(\frac{\pi}{2}\epsilon\right)=\sin\zeta=\frac{\kappa_{\max}}{\sqrt{1+\kappa_{\max}^2}}\ge0.9999\tag{12}$$

or $\kappa_{\max}\ge70.7054$. Hence, to keep the maximum gate error for a single qubit gate below the error threshold of 10^{-4}, for example, we would have to be able to make the energy splitting $\Delta\omega$ (the controllable parameter) at least 71 greater than the fixed coupling d, even if there were no other sources of error. If a controlled-NOT (CNOT) gate is implemented using the Cartan decomposition [Eq. (1)] with $(\alpha_1,\alpha_2,\alpha_3)=(\pi/4,\pi/4,0)$ and $U_1=U_1^{(1)}\otimes U_1^{(2)}$, $U_2=U_2^{(1)}\otimes U_2^{(2)}$, $K_x=K_x^{(1)}\otimes K_x^{(2)}$, $K_y=K_y^{(1)}\otimes K_y^{(2)}$, where

$$K_x^{(1)}=K_x^{(2)}=U_x(\pi),\tag{13a}$$

$$K_y^{(1)}=K_y^{(2)}=U_x(\pi)U_z(\pi),\tag{13b}$$

$$U_1^{(1)}=U_2^{(1)}=U_z(1.75\pi),\tag{13c}$$

$$U_1^{(2)}=U_x(0.5\pi)U_z(1.5\pi)U_x(1.5\pi),\tag{13d}$$

$$U_2^{(2)}=U_z(1.5\pi)U_x(0.5\pi),\tag{13e}$$

then assuming that our z rotations $U_z^\epsilon(\beta)$ are really rotations about the tilted axis $\tilde{Z}=X\sin(\frac{\pi}{2}\epsilon)+Z\cos(\frac{\pi}{2}\epsilon)$, shows that the fidelity of the CNOT gate will be <0.9999 unless the rotation axis angle error is less than about 0.6%, or $\kappa_{\max}\ge100$, even if the entanglement-generating Ising-coupling terms are perfect and there are no other sources of error such as decoherence. In practice, other sources of error would mean that the error resulting from the rotation axis misalignment would have to be much smaller, and thus $\kappa_{\max}$ much bigger, for the total errors to remain below the error threshold. Also note that for $\kappa_{\max}=1$ the rotation axis angle error is 50%, and the maximum single qubit gate error is $1-\cos(\pi/4)$, almost 30%, and the error for a CNOT gate implemented using the Cartan decomposition above with unoptimized single qubit gates jumps to over 50%, assuming no errors in the Ising terms.

III. OPTIMIZED EULER DECOMPOSITION

The previous section shows that accurate single qubit gates are crucial, and even small deviations of the experimentally accessible single qubit Hamiltonians from orthogonality are problematic, not to mention situations where the experimentally accessible Hamiltonians are far from orthogonal. It is also known that *any* local unitary operation, in principle, can be generated exactly by performing a sequence of complex rotations about any two (fixed) Hamiltonians H_1 and H_2 that generate $\mathfrak{su}(2)$, i.e., satisfy $[H_1,H_2]\neq0$. Various Lie group decompositions have been considered for the related problem of implementing local qubit operations exactly in the presence of various types of fixed drift terms [28]. Ideally, however, we would like a simple explicit algorithm to calculate an optimal sequence of rotations given a fixed set of Hamiltonians (rotation axes) and an arbitrary local gate.

In the following we consider general decompositions of SO(3) instead of SU(2) using the equivalence between SU(2) and SO(3) (modulo ± 1). The advantage of considering SO(3) is that it is easier to visualize rotations in $\mathbb{R}^3$ than complex rotations in SU(2). As a brief reminder we recall that any quantum state of a two-level system can be represented by a density operator

$$\rho = \rho(r,\theta,\phi) = \frac{1}{2}\begin{pmatrix} 1 + r^2\cos\theta & r^2 e^{-i\phi}\sin\theta \\ r^2 e^{i\phi}\sin\theta & 1 - r^2\cos\theta \end{pmatrix} \tag{14}$$

with $0 \le \theta \le \pi$, $0 \le \phi \le 2\pi$, and $0 \le r \le 1$, and we can define a unique mapping between density operators ρ of constant purity $\mathrm{Tr}[\rho^2] = \frac{1}{2}(1+r^2)$ and points on a sphere of radius r in $\mathbb{R}^3$ by

$$\rho(r,\theta,\phi) \mapsto \mathbf{s}(r,\theta,\phi) = r\begin{pmatrix} \sin\theta\cos\phi \\ \sin\theta\sin\phi \\ \cos\theta \end{pmatrix}. \tag{15}$$

The evolution of ρ under a constant Hamiltonian H then corresponds to a rotation of the Bloch vector $\mathbf{s}$ about the unit axis $\hat{\mathbf{n}} = \Omega^{-1}\mathbf{d}$ with the constant angular velocity $\Omega = \|\mathbf{d}\|$, as defined in Sec. II. Given two Hamiltonians H_1 and H_2 we calculate the corresponding normalized Bloch vectors $\hat{\mathbf{h}}$ and $\hat{\mathbf{g}}$ and note that the angle between the rotation axes is given by

$$\zeta = \arccos(\hat{\mathbf{h}} \cdot \hat{\mathbf{g}}), \tag{16}$$

and $\zeta \neq 0$ if and only if $[H_1, H_2] \neq 0$.

Any target operator $W(\alpha,\beta,\gamma) \in \mathrm{SU}(2)$ is equivalent (modulo ± 1) to a rotation $R(a,b,c) \in \mathrm{SO}(3)$ acting on the Bloch vector $\mathbf{s}$ with $a = \frac{1}{2}\alpha$, $b = \frac{1}{2}(\beta+\gamma)$ and $c = \frac{1}{2}(\beta-\gamma)$, and we have explicitly

$$R(a,b,c) = \begin{pmatrix} -b_1c_1 + a_2b_2c_2 & b_2c_1 + a_2b_1c_2 & -a_1c_2 \\ -b_1c_2 - a_2b_2c_1 & b_2c_2 - a_2b_1c_1 & a_1c_1 \\ a_1b_2 & a_1b_1 & a_2 \end{pmatrix}, \tag{17}$$

where $a_1 = \sin(a)$, $a_2 = \cos(a)$, and similarly for b and c.

Proposition. Any rotation $R \in \mathrm{SO}(3)$ about an arbitrary axis in $\mathbb{R}^3$ can be decomposed in a series of rotations about two (nonidentical) fixed rotation axes $\hat{\mathbf{h}}$ and $\hat{\mathbf{g}}$ in $\mathbb{R}^3$ as follows:

$$R = \begin{cases} R_{\hat{\mathbf{h}}}(\epsilon_3 + \epsilon_2) R_{\hat{\mathbf{g}}}(\epsilon_1) R_{\hat{\mathbf{h}}}(\epsilon_0), & p = 0 \\ R_{\hat{\mathbf{h}}}(\epsilon_3) X^{p-1} R_{\hat{\mathbf{g}}}(\pi) R_{\hat{\mathbf{h}}}(\tilde{\epsilon}_2) R_{\hat{\mathbf{g}}}(\epsilon_1) R_{\hat{\mathbf{h}}}(\epsilon_0), & p > 0 \end{cases}, \tag{18}$$

where the parameters p, ϵ_0, ϵ_1, ϵ_2, and ϵ_3 are given explicitly in Algorithm 1, and $X = R_{\hat{\mathbf{g}}}(\pi) R_{\hat{\mathbf{h}}}(\pi)$, $\tilde{\epsilon}_2 = \epsilon_2 + \pi$.

We would like emphasize here that the important part from an application point of view is not the existence of a general decomposition of the form (18), which was predicted by [29] and shown in [30], but the simple Algorithm 1 to compute the Euler angles $\epsilon = (\epsilon_0, \ldots, \epsilon_{2p+2})$ in the decomposition based on analytical formulas. In most cases the Euler angles in decompositions about nonorthogonal rotation axes can only be determined numerically using optimization techniques [31], but in this case we are in the fortunate position that we can derive relatively simple analytic formulas for all Euler angles.

Before we discuss the derivation of this result and the algorithm, we should briefly justify the use of the expression "optimized" Euler angles in the title. The factorization (18) shows that in general $2(p-1)+5 = 2p+3$ rotations are necessary, and for $\theta_f \le \pi$ the maximum number of steps is $2p+3 \le \lceil \frac{\pi}{\zeta} \rceil + 1$, which is equal to the order of generation of SO(3), which is $k = \lceil \frac{\pi}{\zeta} \rceil + 1$ according to Lowenthal's criterion [29]. This means that the decomposition is optimal in the sense that we achieve unit fidelity, and that we cannot generate arbitrary rotations using rotations about the fixed axes $\hat{\mathbf{h}}$ and $\hat{\mathbf{g}}$ in fewer steps in general [34]. Optimality in terms of the number of rotation steps is often related to time optimality as more rotation steps generally will take longer to complete, although time optimality is not guaranteed. For instance, if rotations about one axis can be implemented much faster than rotations about the other then a sequence that requires more steps but fewer slow rotations by larger angles may be faster to implement. Also, it should be noted that while the decomposition (18) generally provides the best way to implement a quantum gate in SU(2) exactly using a minimal number of rotations about two fixed axes, we may be able to implement a particular gate substantially faster if we can dynamically vary the rotation axes continuously. For example, consider a system with Hamiltonian $H = \frac{d}{2}(\sigma_x + \kappa\sigma_z)$. If we can temporally vary $\kappa(t)$ to take any value in the range $[0, \kappa_{\max}]$ rather than two fixed values, e.g., 0 and $\kappa_{\max}$, then we may be able to implement a particular gate faster by numerically optimizing $\kappa(t)$ instead of using the optimized Euler angle decomposition. The attractivity of the generalized Euler decomposition lies in its simplicity. It is a simple "bang-bang" control scheme that can be used to achieve unit fidelity when we have limited control and cannot (or do not wish to) implement complicated temporal control field profiles $\kappa(t)$.

Algorithm 1. Calculate generalized Euler angles for decomposition of arbitrary $R \in \mathrm{SO}(3)$.

Input: $R \in \mathrm{SO}(3)$, unit vectors $\hat{\mathbf{h}}, \hat{\mathbf{g}} \in \mathbb{R}^3$, $\hat{\mathbf{h}} \neq \pm\hat{\mathbf{g}}$.
Output: Euler angles $\epsilon = (\epsilon_0, \ldots, \epsilon_{2p+2})$
$\zeta = \arccos(\hat{\mathbf{h}} \cdot \hat{\mathbf{g}})$
$(\theta_{af}, \phi_{af}) = \mathbf{Polar}(R\hat{\mathbf{h}}, \hat{\mathbf{h}}, \hat{\mathbf{g}})$
$p = \lceil \theta_{af}/2\zeta \rceil$
if $p > 0$
  $p = p - 1$
end
$\theta = \theta_{af} - 2\zeta p$
$\epsilon_1 = -\arccos[\cot\zeta \tan(\theta/2)]$
$\epsilon_2 = -\arccos[(-\cos^2\zeta + \cos\theta)/\sin^2\zeta]$
$\epsilon_3 = \phi_{af}$
$T_p = [R_{\hat{\mathbf{h}}}(\pi) R_{\hat{\mathbf{g}}}(\pi)]^p$

$S_1 = R_{\hat{\mathbf{g}}}(-\epsilon_1) R_{\hat{\mathbf{h}}}(-\epsilon_2) T_p R_{\hat{\mathbf{h}}}(-\epsilon_3)$
$(\theta_{b1}, \phi_{b1}) = \mathbf{Polar}[S_1 R R_{\hat{\mathbf{y}}}(\pi/2)\hat{\mathbf{h}}, \hat{\mathbf{h}}, \hat{\mathbf{g}}]$
$\epsilon_0 = \phi_{b1}$
if $p=3$
  $\epsilon = [\epsilon_0, \epsilon_1, \epsilon_2 + \epsilon_3]$
else
  $\epsilon = [\epsilon_0, \epsilon_1, \epsilon_2 + \pi, \underbrace{\pi, \ldots, \pi}_{2p-1}, \epsilon_3]$
end
$\epsilon = \epsilon + 2\pi \lfloor (2\pi - \epsilon)/(2\pi) \rfloor$

Algorithm 2 (Polar). Compute polar coordinates of $\hat{\mathbf{a}}$ with respect to orthogonal frame induced by $\hat{\mathbf{h}}$ and $\hat{\mathbf{g}}$.

Input: unit vectors $\hat{\mathbf{a}}, \hat{\mathbf{h}}, \hat{\mathbf{g}} \in \mathbb{R}^3$
Output: polar coordinates (θ, ϕ) of $\hat{\mathbf{a}}$
  $\hat{\mathbf{z}} = \hat{\mathbf{h}}$
  $\mathbf{y} = \hat{\mathbf{h}} \times \hat{\mathbf{g}}$
  $\hat{\mathbf{y}} = \mathbf{y}/\|\mathbf{y}\|$
  $\hat{\mathbf{x}} = \hat{\mathbf{y}} \times \hat{\mathbf{h}}$
  $\theta = \arccos(\hat{\mathbf{a}} \cdot \hat{\mathbf{z}})$
  $\phi = \arctan(\hat{\mathbf{a}} \cdot \hat{\mathbf{y}}, \hat{\mathbf{a}} \cdot \hat{\mathbf{x}})$

The derivation of the algorithm is based on steering of a state represented by a vector $\mathbf{s}_0 \in \mathbb{R}^3$ of length r to another state $\mathbf{s}_f \in \mathbb{R}^3$ the same distance from the origin using only rotations about the two fixed rotation axes given by the unit vectors $\hat{\mathbf{h}}$ and $\hat{\mathbf{g}}$. An algorithm and detailed explanation how to move from one point on the sphere (Fig. 1) to another though a sequence of rotations about two fixed axes $\hat{\mathbf{h}}$ and $\hat{\mathbf{g}}$ is presented in Appendix A. However, this algorithm on its own is not sufficient for gate engineering as a single point and its image on the unit sphere in $\mathbb{R}^3$ are not sufficient to uniquely determine a rotation in $R \in \mathrm{SO}(3)$. Rather, we need at least two (nonantipodal) points and their images to fix R.

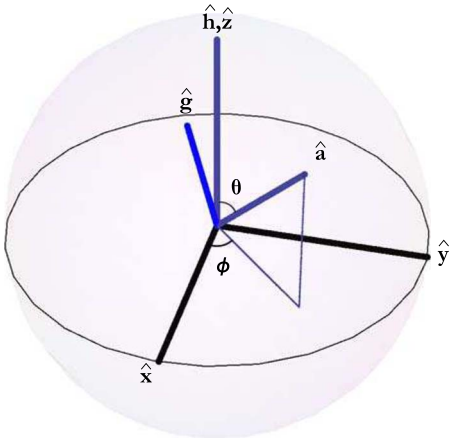

FIG. 1. (Color online) Sphere with arbitrary rotation axes, respective coordinate system and an arbitrary vector $\hat{\mathbf{a}}$ (angles θ and ϕ).

This may seem surprising as the parametrization (2) for a unitary operator $W \in \mathrm{SU}(2)$ shows that the image $W|\psi\rangle$ of a single Hilbert space vector $|\psi\rangle$ is sufficient to fix all three parameters. The corresponding real rotation (17), however, cannot be fully determined by the image of a single Bloch vector. Rather the mapping of a single point in $\mathbb{R}^3$ defines a one-parameter family of elements of SO(3), and a second (nonantipodal) point and its image are required to fix all three parameters a, b, c of R. The reason for this apparent discrepancy is that when we transform from complex Hilbert space vectors $|\psi\rangle$ to density matrices $\rho = |\psi\rangle\langle\psi|$ the information about the global phase of the initial and final states, which helps fix W uniquely, is lost.

Any pair of nonantipodal initial points $(\hat{\mathbf{a}}_0, \hat{\mathbf{b}}_0)$ and their images $(\hat{\mathbf{a}}_f, \hat{\mathbf{b}}_f)$, are sufficient, but it is convenient to choose the initial points to be the orthogonal set of initial states

$$\hat{\mathbf{a}}_0 = \hat{\mathbf{h}} = (0,0), \tag{19a}$$

$$\hat{\mathbf{b}}_0 = R_{\hat{\mathbf{y}}}\left(\frac{\pi}{2}\right)\hat{\mathbf{a}}_0 = \left(\frac{\pi}{2}, 0\right), \tag{19b}$$

where the pairs (θ, ϕ) are the polar coordinates

$$\theta = \theta(\hat{\mathbf{a}}) = \arccos(\hat{\mathbf{a}} \cdot \hat{\mathbf{z}}), \tag{20a}$$

$$\phi = \phi(\hat{\mathbf{a}}) = \arctan(\hat{\mathbf{a}} \cdot \hat{\mathbf{y}}, \hat{\mathbf{a}} \cdot \hat{\mathbf{x}}) \tag{20b}$$

of the unit vectors $\mathbf{a}_0$ and $\mathbf{b}_0$ with respect to the rectangular coordinate system $(\hat{\mathbf{x}}, \hat{\mathbf{y}}, \hat{\mathbf{z}})$ defined by

$$\hat{\mathbf{z}} = \hat{\mathbf{h}}, \quad \hat{\mathbf{y}} = \frac{\hat{\mathbf{h}} \times \hat{\mathbf{g}}}{\|\hat{\mathbf{h}} \times \hat{\mathbf{g}}\|}, \quad \hat{\mathbf{x}} = \hat{\mathbf{y}} \times \hat{\mathbf{h}}. \tag{21}$$

and the four-quadrand arctangent is

$$\arctan(y,x) = \begin{cases} \arctan|y/x| & x \geq 0, \ y \geq 0 \\ \pi - \arctan|y/x| & x < 0, \ y \geq 0 \\ \pi + \arctan|y/x| & x < 0, \ y < 0 \\ 2\pi - \arctan|y/x| & x \geq 0, \ y < 0. \end{cases} \tag{22}$$

Then we compute the polar coordinates of the corresponding images under the target rotation R

$$\hat{\mathbf{a}}_f = R\hat{\mathbf{a}}_0 = (\theta_{af}, \phi_{af}), \tag{23a}$$

$$\hat{\mathbf{b}}_f = R\hat{\mathbf{b}}_0 = (\theta_{bf}, \phi_{bf}). \tag{23b}$$

and use the state transfer algorithm (Algorithm 3) to calculate S_1, the series of rotations that steer $\hat{\mathbf{a}}_f$ to $\hat{\mathbf{a}}_0$,

$$S_1 = R_{\hat{\mathbf{g}}}(-\epsilon_1) R_{\hat{\mathbf{h}}}(-\epsilon_2) T^p R_{\hat{\mathbf{h}}}(-\phi_{af}),$$

where $T = R_{\hat{\mathbf{h}}}(\pi) R_{\hat{\mathbf{g}}}(\pi)$ and p is the largest integer strictly less than $\theta_{af}/2\zeta$, i.e., $p = \lceil \theta_{af}/2\zeta \rceil - 1$. The generalized Euler angles ϵ_1 and ϵ_2 can be obtained by inserting $\theta_f = 0$ and $\theta_0 = \theta_{af} - 2p\zeta \neq 0$ into subroutine PR2 (see Appendix B)

$$\epsilon_2 = -\arccos\left[\cot\zeta \tan\left(\frac{\theta_{af} - 2p\zeta}{2}\right)\right], \tag{24a}$$

TABLE I. Optimized Euler angles (in units of π) for various single qubit gates and different values of κ. $\epsilon(\tilde{H}_1)$ indicates a rotation by ϵ about the normalized axis $\tilde{H}_1$. $\mathcal{E}_0$ is the gate error that results if the standard Euler angles for $\kappa=\infty$ are used. The gate errors using the optimized Euler angles truncated to four decimal digits are $<3\times10^{-9}$ for all gates, and can be made arbitrarily small by increasing the number of significant digits of the Euler angles.

	κ	$\mathcal{E}_0$ (%)	$\epsilon(\tilde{H}_1)$	$\epsilon(\tilde{H}_2)$	$\epsilon(\tilde{H}_1)$	$\epsilon(\tilde{H}_2)$
S_2	∞	0	0	1.7500	0	
	100	0.0007	0.0013	1.7500	0.0013	
	50	0.0029	0.0026	1.7499	0.0026	
	10	0.0727	0.0132	1.7487	0.0132	
	5	0.2844	0.0264	1.7448	0.0264	
	1	4.2893	0.1359	1.6359	0.1359	
S	∞	0	0	1.5000	0	
	100	0.0025	0.0032	1.5000	0.0032	
	50	0.0100	0.0064	1.4999	0.0064	
	10	0.2481	0.0319	1.4968	0.0319	
	5	0.9710	0.0641	1.4873	0.0641	
	1	14.6446	0.5000	1	0.5000	
U_{Had}	∞	0	1.5000	1.5000	1.5000	
	100	0.0025	1.5032	1.5000	1.5032	
	50	0.0100	1.5064	1.4999	1.5064	
	10	0.2481	1.5319	1.4968	1.5319	
	5	0.9709	1.5641	1.4873	1.5641	
	1	14.6442	0	1	0	
$U_1^{(2)}$	∞	0	0.5000	1.5000	1.5000	
	100	0.0025	0.5032	1.5000	1.5032	
	50	0.0100	0.5064	1.4999	1.5064	
	10	0.2481	0.5319	1.4968	1.5319	
	5	0.9709	0.5641	1.4873	1.5641	
	1	14.6443	1	1	0	
$U_2^{(2)}$	∞	0	0	1.5000	0.5000	
	100	0.0025	0.0032	1.5000	0.5032	
	50	0.0100	0.0064	1.4999	0.5064	
	10	0.2481	0.0319	1.4968	0.5319	
	5	0.9709	0.0641	1.4873	0.5641	
	1	14.6445	0.5000	1	1	
$K_y^{(1)}$	∞	0	0	0	1	1
	100	0.0050	0.5000	1.9936	0.5000	1
	50	0.0200	0.5001	1.9873	0.5001	1
	10	0.4963	0.5032	1.9362	0.5032	1
	5	1.9419	0.5127	1.8718	0.5127	1
	1	29.2893	1	1	1	1

$$\epsilon_1 = -\arccos\left[\frac{-\cos^2\zeta + \cos(\theta_{af} - 2p\zeta)}{\sin^2\zeta}\right]. \quad (24b)$$

Since $S_1\hat{\mathbf{b}}_f = (\frac{\pi}{2}, \phi_{b1})$ and $\hat{\mathbf{b}}_0$ are unit vectors with the same θ-angle ($\theta = \frac{\pi}{2}$), the same series of rotations preserves the distance between the points, hence

$$\hat{\mathbf{b}}_0 = R_{\hat{\mathbf{h}}}(-\phi_{b1}) S_1 \hat{\mathbf{b}}_f.$$

The $R_{\hat{\mathbf{h}}}$ rotations leave $\hat{\mathbf{a}}_0$ unchanged and we have

$$\hat{\mathbf{a}}_0 = R_{\hat{\mathbf{h}}}(-\phi_{b1}) S_1 \hat{\mathbf{a}}_f.$$

Thus $R = S_1^{-1} R_{\hat{\mathbf{h}}}(\phi_{b1})$ and we have the decomposition

$$R = R_{\hat{\mathbf{h}}}(\epsilon_3) X^p R_{\hat{\mathbf{h}}}(\epsilon_2) R_{\hat{\mathbf{g}}}(\epsilon_1) R_{\hat{\mathbf{h}}}(\epsilon_0), \quad (25)$$

where $X = T^{-1} = R_{\hat{\mathbf{g}}}(\pi) R_{\hat{\mathbf{h}}}(\pi)$ and $\epsilon_0 = \phi_{b1}$, $\epsilon_3 = \phi_{af}$ and ϵ_1, ϵ_2 as in Eq. (24). If $p > 1$ we can combine the two subsequent $\hat{\mathbf{h}}$ rotations, while for $p = 0$, $T^p = \mathbf{I}$, thus the optimal decomposition is

$$R = \begin{cases} R_{\hat{\mathbf{h}}}(\epsilon_3 + \epsilon_2) R_{\hat{\mathbf{g}}}(\epsilon_1) R_{\hat{\mathbf{h}}}(\epsilon_0), & p = 0 \\ R_{\hat{\mathbf{h}}}(\epsilon_3) X^{p-1} R_{\hat{\mathbf{g}}}(\pi) R_{\hat{\mathbf{h}}}(\tilde{\epsilon}_2) R_{\hat{\mathbf{g}}}(\epsilon_1) R_{\hat{\mathbf{h}}}(\epsilon_0), & p > 0 \end{cases}$$

with $\tilde{\epsilon}_2 = \epsilon_2 + \pi$, which completes the proof.

IV. APPLICATIONS

To apply the results in the previous section to implement a quantum gate

$$U = \exp[i\Phi(n_x\sigma_x + n_y\sigma_y + n_z\sigma_z)] \quad (26)$$

given the Hamiltonians

$$H_1 = \frac{d}{2}\sigma_x, \quad H_2 = \frac{d}{2}(\sigma_x + \kappa\sigma_z), \quad (27)$$

we identify the normalized Hamiltonians $\tilde{H}_1 = \sigma_x$ and $\tilde{H}_2 = (\sigma_x + \kappa\sigma_z)/\sqrt{1+\kappa^2}$ with the unit vectors $\hat{\mathbf{h}} = (1,0,0)^T$ and $\hat{\mathbf{g}} = (1,0,\kappa)^T/\sqrt{1+\kappa^2}$, respectively, and use Algorithm 1 to decompose the corresponding SO(3) representation of the target operator U

$$A = \exp[\Phi(n_x R_x + n_y R_y + n_z R_z)], \quad (28)$$

where R_x, R_y and R_z are the rotation generators

$$R_x = \begin{pmatrix} 0 & 0 & 0 \\ 0 & 0 & 2 \\ 0 & -2 & 0 \end{pmatrix}, R_y = \begin{pmatrix} 0 & 0 & -2 \\ 0 & 0 & 0 \\ 2 & 0 & 0 \end{pmatrix}, R_z = \begin{pmatrix} 0 & 2 & 0 \\ -2 & 0 & 0 \\ 0 & 0 & 0 \end{pmatrix}.$$

Table I shows the optimized Euler angle decomposition results for the gates $S = \exp(i\frac{\pi}{4}\sigma_z)$, $S_2 = \exp(i\frac{\pi}{8}\sigma_z)$,

$$U_{\mathrm{Had}} = \exp\left[i\frac{\pi}{2\sqrt{2}}(\sigma_x + \sigma_z)\right] \quad (29)$$

as well as for the single qubit gates [Eq. (12)] required to implement a CNOT gate via the Cartan decomposition (1). Gates that require only σ_x rotations have been omitted as they are trivial to implement with the given Hamiltonians. Using the optimized Euler angles rounded to four significant digits, the gate errors for all single qubit gates in the table, as well as the CNOT gate, are below 3×10^{-9} for values of κ shown, while the gate errors using the standard Euler angles increase to almost 30% for K_y and $\kappa = 1$. The error for the resulting CNOT gate increases from $\approx 10^{-4}$ for $\kappa = 100$ to over 51% for $\kappa = 1$. Also note that the penalty for nonorthogonal Hamiltonians in terms of the number of rotation steps required is actually rather small unless κ is very small. Indeed for $\kappa \geq 1$ all of the elementary gates in the table can be implemented in at most four steps, and for $\kappa > 1$, this is indeed the maximum number of steps required for any single qubit gate. To see this recall that Lowenthal's criterion guarantees that the maximum number of steps in the decomposition of any single qubit gates is

$$K = \left\lceil \frac{\pi}{\zeta} \right\rceil + 1 = \left\lceil \frac{\pi}{\arccos[(1+\kappa^2)^{-1/2}]} \right\rceil + 1, \quad (30)$$

which yields $K = 3$ for $\kappa = \infty$ and $K = 4$ for $1 < \kappa < \infty$, $K = 5$ for $\kappa = 1$, $K = 6$ for $\sqrt{[\cos(\pi/5)]^{-2} - 1} < \kappa < 1$, and so forth.

V. CONCLUSIONS

The Euler decomposition of unitary operators in SU(2) is widely used to implement single qubit gates by decomposing them into products of rotations about two orthogonal axes determined by fixed Hamiltonians. The approach can be problematic however as experimentally accessible Hamiltonians in many cases may not be orthogonal. Depending on the situation, in some cases the Hamiltonians can be made almost orthogonal, while in others the constraints may be far more severe. In either case, however, lack of orthogonality of the underlying Hamiltonians leads to errors in the gates implemented, and even small errors can propagate. A rotation axis angle error of even 1% results in single qubit gate errors above the error threshold of 10^{-4} even if there are no other sources of errors, and the single qubit errors compound and lead to even larger errors for two-qubit gates. Such systematic errors can easily be corrected, however, by adapting the Euler decomposition to the actual Hamiltonians available.

We have presented an explicit algorithm to calculate the optimized Euler angles for any single qubit gate and two arbitrary fixed Hamiltonians, and shown that we can substantially improve single and two-qubit gate fidelities by using optimized rather than standard Euler angles. The idea is attractive because the computational overhead to calculate the optimized Euler angles is minimal and the implementation is no more demanding than standard geometric control, i.e., no additional resources are required. There is a small price to pay in terms of an increase in the number of rotation steps required to implement a particular gate, but unless the maximum angle between the experimentally accessible Hamiltonians is very small, this increase is very slight, e.g., from at

most three steps for orthogonal Hamiltonians to four for Hamiltonians with angle ζ greater than 45° and five if $\zeta = 45°$. For a model Hamiltonian $H(\kappa)=\frac{d}{2}(\sigma_x+\kappa\sigma_z)$ with a fixed coupling parameter d, this condition is satisfied if the energy level splitting can be made at least as large as the tunneling energy d, or $\kappa=1$, whereas the standard Euler decomposition would require $\kappa\to\infty$, or energy level splittings that are orders of magnitude greater than the tunneling energy d to achieve near-orthogonal Hamiltonians.

Overall, the overhead in terms of complexity of the pulse sequences is small compared to alternative ways to correct for rotation axis errors, such as composite pulse sequences, and this overhead seems acceptable, considering that relaxing the need to be able to perform rotations about orthogonal axes may allow for substantial simplifications of the underlying architectures. Another source of overhead of the technique is the need for initial characterization of the Hamiltonians. It must also be stressed that optimized Euler angles are designed to minimize errors for a single system. They cannot compensate for ensemble errors, i.e., errors arising from the fact that individual systems in a large ensemble may experience different fields and thus different effective rotations. However, the approach is an effective way to improve gate fidelities for nonensemble systems with nonideal Hamiltonians.

Further work is necessary to extend the results to higher-dimensional systems. Another issue is that different gates require different amounts of time to implement. This is not a problem for a single system but would be for a large register if one wants to implement gates on different qubits simultaneously. Here we have only used two fixed Hamiltonians with a fixed angle between them. In many cases, however, we may be able to vary the controllable parameter continuously up to some maximum value. An interesting question in this regard is whether we can exploit the (limited) variation in the tilt angle to design simple geometric controls that allow us to implement arbitrary gates in a fixed amount of time.

ACKNOWLEDGMENTS

S.G.S. acknowledges support from EPSRC ARF Grant No. EP/D07195X/1, European Union Knowledge Transfer Programme Grant No. MTDK-CT-2004-509223, Hitachi and NSF Grant No. PHY05-51164. G.C. is supported by Grant No. VZ3407391 of the Ministry of Education, Youth and Sports of the Czech Republic. C.D. acknowledges support of the Program of the Cultural Exchanges-2008 between the Czech and the Hellenic Republic.

APPENDIX A: STATE TRANSFER ALGORITHM

The objective of state transfer is to steer the system from a known initial state $\mathbf{s}_0=(r,\theta_0,\phi_0)$ on a sphere of radius r to a target state $\mathbf{s}_f=(r',\theta_f,\phi_f)$. With unitary control only states on the same sphere as the initial state are accessible by performing a sequence of rotations about the axes $\hat{\mathbf{h}}$ and $\hat{\mathbf{g}}$, respectively. We shall assume $r=1$, noting that the sequence of rotations that steers the normalized initial state $\hat{\mathbf{a}}_0$ to the normalized target state $\hat{\mathbf{a}}_f$ steers $\mathbf{s}_0$ to $\mathbf{s}_f$ if they lie on the same sphere of radius r, and to a state $\mathbf{s}_f'$ that is as close to the target state as we can get with unitary control if $r\neq r'$.

A general strategy to get from $\mathbf{s}_0$ to $\mathbf{s}_1$ with a minimum number of rotations about the axes $\hat{\mathbf{h}}=\hat{\mathbf{z}}$ and $\hat{\mathbf{g}}=(\sin\zeta,0,\cos\zeta)^T$, following [30] and earlier work [29,32,33], is to rotate the initial state by a suitable angle about either axis to map it to a point on the great circle in the $\hat{\mathbf{x}},\hat{\mathbf{z}}$ plane, followed by a sequence of π rotations, alternating about the $\hat{\mathbf{h}}$ and $\hat{\mathbf{g}}$ axis, until the angle θ' of the current state differs by less than 2ζ from the θ_f of the target state, i.e., we are within direct reach of the target state, followed by a final rotation by a suitable angle about the same axis we started with. By Lowenthal's criterion any state can be reached from any other state in at most $k+1$ steps, k being the smallest integer $\geq\frac{\pi}{\zeta}-1$ [29], and for $\zeta=\frac{\pi}{2}$ at most two steps are required.

Based on this idea, we can derive an explicit algorithm for calculating the generalized Euler angles of an optimal decomposition given the angle α between the rotation axes $\hat{\mathbf{h}}$ and $\hat{\mathbf{g}}$, and the relative coordinates (θ_0,ϕ_0) and (θ_f,ϕ_f) of the initial and final state. Assume $\theta_0>\theta_f$ and $\zeta<\pi/2$. If $\theta_0-\theta_f\leq 2\zeta$ then we can get from $(\theta_0,0)$ to $(\theta_f,0)$ in two steps, either by rotating $(\theta_0,0)$ around $\hat{\mathbf{g}}$ by an angle θ, followed by a rotation about $\hat{\mathbf{h}}$ by an angle ϕ (Subroutine PR1), or by a rotation around $\hat{\mathbf{h}}$ by an angle ϕ, followed by a rotation around $\hat{\mathbf{g}}$ by an angle θ (Subroutine PR2). If $\theta_0-\theta_f>2\zeta$ then we move from the initial point to a point with $\theta_0'-\theta_f\leq 2\zeta$ via a sequence of π rotations around axes $\hat{\mathbf{g}}$ and $\hat{\mathbf{h}}$ as described before. If $\zeta\leq\pi/2$ but $\theta_0<\theta_f$ then we exchange the initial and final points, apply the algorithm and finally reverse the sequence of rotations. If $\zeta>\pi/2$ we set $(\theta_1,\phi_1)=(\pi-\theta_0,\phi_0)$, $(\theta_2,\phi_2)=(\pi-\theta_f,\phi_f)$, and $\tilde{\zeta}=\pi-\zeta$ and apply the algorithm.

The algorithm returns a list of pairs $(\epsilon,\hat{\mathbf{r}})$, where $\epsilon\in[0,\pi]$ is a generalized Euler angle and $\hat{\mathbf{r}}=\hat{\mathbf{h}}$ or $\hat{\mathbf{r}}=\hat{\mathbf{g}}$ indicates the rotation axis, which defines the necessary sequence of the rotations. E.g., if $\theta_0>\theta_f$, $\zeta<\frac{\pi}{2}$ and routine PR1 was used, then

$$\mathbf{s}(\theta_f,\phi_f)=R_{\hat{\mathbf{h}}}(\phi_f)R_{\hat{\mathbf{h}}}(\phi)R_{\hat{\mathbf{g}}}(\theta)T^pR_{\hat{\mathbf{h}}}(-\phi_0)\mathbf{s}(\theta_0,\phi_0). \tag{A1}$$

where the angles ϕ and θ are given by

$$\cos\phi=\frac{\sin\theta_0-\cot\zeta(\cos\theta_f-\cos\theta_0)}{\sin\theta_f}, \tag{A2a}$$

$$\cos\theta=\frac{-\cos\zeta\cos(\zeta-\theta_0)+\cos\theta_f}{\sin\zeta\sin(\zeta-\theta_0)}. \tag{A2b}$$

Similarly, if PR2 was used

$$\mathbf{s}(\theta_f,\phi_f) = R_{\hat{\mathbf{h}}}(\phi_f)R_{\hat{\mathbf{g}}}(\theta)R_{\hat{\mathbf{h}}}(\phi)T^pR_{\hat{\mathbf{h}}}(-\phi_0)\mathbf{s}(\theta_0,\phi_0), \tag{A3}$$

where the angles ϕ and θ are determined by

$$\cos\phi = \frac{\sin\theta_f - \cot\zeta(\cos\theta_0 - \cos\theta_f)}{\sin\theta_0}, \tag{A4a}$$

$$\cos\theta = \frac{-\cos\zeta\cos(\zeta-\theta_f)+\cos\theta_0}{\sin\zeta\sin(\zeta-\theta_f)}. \tag{A4b}$$

The procedures PR1 and PR2 are described in Appendix B, and in both cases we have

$$T^p = \underbrace{R_{\hat{\mathbf{h}}}(\pi)R_{\hat{\mathbf{g}}}(\pi)\ldots R_{\hat{\mathbf{h}}}(\pi)R_{\hat{\mathbf{g}}}(\pi)}_{2\mathrm{p\ rotations}}. \tag{A5}$$

The minimal number of steps can be calculated explicitly. If $\theta_0=\theta_f$ then only a single rotation about $\hat{\mathbf{h}}$ is required, otherwise the minimal number of steps to get from (θ_0,ϕ_0) to (θ_f,ϕ_f) starting with a rotation about $\hat{\mathbf{h}}$ is $N=2p+2+\Theta(q)$, where $\Theta(q)=1$ for $q>0$ and 0 otherwise,

$$p = \mathrm{int}[(\theta_0-\theta_f)/2\zeta], \tag{A6a}$$

$$q = \cos\theta_f - [\tan\zeta(\sin\bar{\theta} - \sin\theta_f\cos\phi_f) + \cos\bar{\theta}], \tag{A6b}$$

and $\bar{\theta}=\theta_0-2p\zeta$. Here, int$(x)$ indicates the integer part of x.

The minimal number of steps to get from (θ_0,ϕ_0) to (θ_f,ϕ_f) starting with a rotation about $\hat{\mathbf{g}}$ is $N'=2+\Theta(\theta'-\theta_f)[2p+1+\Theta(q)]$, where

$$p = \mathrm{int}[(\theta'-\theta_f)/2\zeta], \tag{A7a}$$

$$q = \cos\theta_f - [\tan\zeta(\sin\bar{\theta} - \sin\theta_f\cos\phi_f) + \cos\bar{\theta}], \tag{A7b}$$

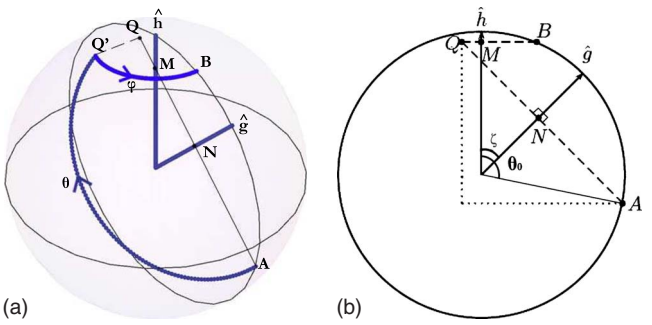

FIG. 2. (Color online) Rotations on the sphere and projection to the x-z plane for subroutine PR1.

with $\theta'=\arccos(\cos\zeta\cos\theta_0+\sin\zeta\sin\theta_0\cos\phi_0)-\zeta$ and $\bar{\theta}=\theta'-2p\zeta$.

Algorithm 3. Calculate sequence of rotations about arbitrary, fixed axes $\hat{\mathbf{h}}$ and $\hat{\mathbf{g}}$ required to move from one point on the unit sphere to another.

Input: (θ_0,ϕ_0), (θ_f,ϕ_f)—polar coordinates of initial and final point with respect to relative coordinate system (21).

Output: List of pairs $(\epsilon,\hat{\mathbf{u}})$, $\hat{\mathbf{u}}\in\{\hat{\mathbf{h}},\hat{\mathbf{g}}\}$ defining rotation steps necessary to get from initial state to final state.

if $\theta_0=\theta_f$ **return** $\{(\phi_f-\phi_0,\hat{\mathbf{h}})\}$
else
  $p=\lfloor(\theta_0-\theta_f)/2\zeta\rfloor$
  $\theta_0=\theta_0-2p\zeta$
  if $\theta_0=\theta_f$ **return**
    $\{(\phi_f,\hat{\mathbf{h}}),\underbrace{(\pi,\hat{\mathbf{g}}),(\pi,\hat{\mathbf{h}}),\ldots(\pi,\hat{\mathbf{g}}),(\pi,\hat{\mathbf{h}})}_{2p\ \mathrm{pairs}},(-\phi_0,\hat{\mathbf{h}})\}$
  else if $\theta_0\le\zeta$ or $(2\zeta-\theta_0\ge0$ and $2\zeta-\theta_0>\theta_f)$
    return
      $\{(\phi_f,\hat{\mathbf{h}}),\underbrace{(\pi,\hat{\mathbf{g}}),(\pi,\hat{\mathbf{h}}),\ldots,(\pi,\hat{\mathbf{g}}),(\pi,\hat{\mathbf{h}})}_{2\mathrm{p\ pairs}},\mathrm{PR2}[\theta_0,\theta_f,\zeta],(-\phi_0,\hat{\mathbf{h}})\}$
    else return
      $\{(\phi_f,\hat{\mathbf{h}}),\underbrace{(\pi,\hat{\mathbf{g}}),(\pi,\hat{\mathbf{h}}),\ldots,(\pi,\hat{\mathbf{g}}),(\pi,\hat{\mathbf{h}})}_{2\mathrm{p\ pairs}},\mathrm{PR1}[\theta_0,\theta_f,\zeta],(-\phi_0,\hat{\mathbf{h}})\}$
    end
  end
end

APPENDIX B: SUBROUTINES PR1 AND PR2

Both procedures take only the θ angles of the initial and final points, θ_0 and θ_f, respectively, and the angle α between the axes $\hat{\mathbf{h}}$ and $\hat{\mathbf{v}}$ as input, assuming that the points have already been shifted to the $\hat{\mathbf{x}}$-$\hat{\mathbf{z}}$ plane.

1. Subroutine PR1

Figure 2 shows that $\|\mathbf{MB}\|=\|\mathbf{MQ}'\|$ and $\|\mathbf{NA}\|=\|\mathbf{NQ}'\|$ and

$$\cos\phi = \frac{|\mathbf{MB}\cdot\mathbf{MQ}'|}{\|\mathbf{MB}\|^2}, \quad \cos\theta = \frac{|\mathbf{NA}\cdot\mathbf{NQ}'|}{\|\mathbf{NA}\|^2}. \tag{B1}$$

Noting that $\mathbf{A}=(\sin\theta_0,0,\cos\theta_0)$ and $\mathbf{Q}'=(q,p,\cos\theta_f)$ for suitable values of p and q, and taking $\mathbf{Q}=(q,0,\cos\theta_f)$ to be the projection of $\mathbf{Q}'$ onto the $\hat{\mathbf{x}}$-$\hat{\mathbf{z}}$ plane, shows

$$\cot\zeta = -\frac{\mathbf{QA}\cdot\hat{\mathbf{x}}}{\mathbf{QA}\cdot\hat{\mathbf{z}}} = \frac{\sin\theta_0 - q}{\cos\theta_0 - \cos\theta_f} \tag{B2}$$

and thus $q=\sin\theta_0-\cot\zeta(\cos\theta_f-\cos\theta_0)$. Noting further that $\mathbf{B}=(\sin\theta_f,0,\cos\theta_f)$ and $\mathbf{M}=(0,0,\cos\theta_f)$, shows that $\mathbf{MQ}'=(q,p,0)$, $\mathbf{MB}=(\sin\theta_f,0,0)$, and therefore

$$\cos\phi = \frac{q\sin\theta_f}{\sin^2\theta_f} = \frac{\sin\theta_0 - \cot\zeta(\cos\theta_f - \cos\theta_0)}{\sin\theta_f}. \tag{B3}$$

Furthermore, we have $\mathbf{N}=r(\sin\zeta,0,\cos\zeta)$ with $r=\cos(\theta_0-\zeta)$ and $|\mathbf{NA}|=\sin(\theta_0-\zeta)$, and

$$\mathbf{NA} = (\sin\theta_0 - r\sin\zeta, 0, \cos\theta_0 - r\cos\zeta),$$

$$\mathbf{NQ}' = (q - r\sin\zeta, p, \cos\theta_0 - r\cos\zeta),$$

$$\mathbf{NA}\cdot\mathbf{NQ}' = (\sin\theta_0 - n_x)(q - n_x) + (\cos\theta_0 - n_z)^2,$$

which after some simplification gives

$$\cos\theta = \frac{-\cos\zeta\cos(\zeta-\theta_0) + \cos\theta_f}{\sin\zeta\sin(\zeta-\theta_0)}. \tag{B4}$$

2. Subroutine PR2

Figure 3 shows that $\|\mathbf{MA}\|=\|\mathbf{MQ}'\|$ and $\|\mathbf{NB}\|=\|\mathbf{NQ}'\|$ and

$$\cos\phi = \frac{|\mathbf{MA}||\mathbf{MQ}'|}{|\mathbf{MA}|^2}, \quad \cos\theta = \frac{|\mathbf{NB}||\mathbf{NQ}'|}{|\mathbf{NB}|^2}. \tag{B5}$$

Noting that $\mathbf{B}=(\sin\theta_f,0,\cos\theta_f)$ and $\mathbf{Q}'=(q,p,\cos\theta_0)$ for suitable p and q as before, shows that

$$\cot\zeta = -\frac{\mathbf{QB}\cdot\hat{\mathbf{x}}}{\mathbf{QB}\cdot\hat{\mathbf{z}}} = -\frac{\sin\theta_f - q}{\cos\theta_f - \cos\theta_0}, \tag{B6}$$

i.e., $q=\sin\theta_f-\cot\zeta(\cos\theta_0-\cos\theta_f)$.

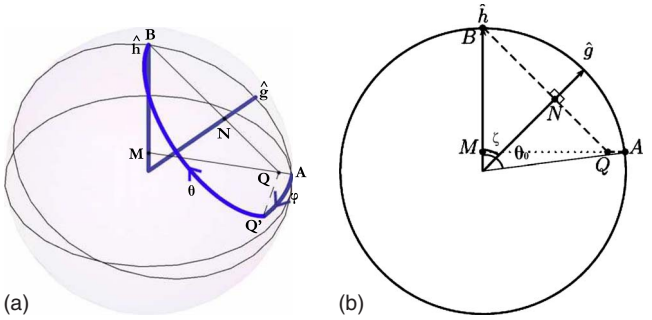

FIG. 3. (Color online) Rotations on the sphere and projection to the x-z plane for subroutine PR2.

Taking $\mathbf{Q}=(q,0,\cos\theta_0)$ to be the projection of $\mathbf{Q}'$ onto the $\hat{\mathbf{x}}\hat{\mathbf{z}}$ plane, and noting that $\mathbf{A}=(\sin\theta_0,0,\cos\theta_0)$ and $\mathbf{M}=(0,0,\cos\theta_0)$ shows that $\mathbf{MQ}'=(q,p,0)$, $\mathbf{MA}=(\sin\theta_f,0,0)$, and thus

$$\cos\phi = \frac{q\sin\theta_0}{\sin^2\theta_0} = \frac{\sin\theta_f - \cot\zeta(\cos\theta_0 - \cos\theta_f)}{\sin\theta_0}. \tag{B7}$$

Furthermore, we have $\mathbf{N}=r(\sin\zeta,0,\cos\zeta)$ with $r=\cos(\theta_f-\zeta)$ and $|\mathbf{NB}|=\sin(\theta_f-\zeta)$, and

$$\mathbf{NB} = (\sin\theta_f - r\sin\zeta, 0, \cos\theta_f - r\cos\zeta),$$

$$\mathbf{NQ}' = (q - r\sin\zeta, p, \cos\theta_0 - r\cos\zeta),$$

$$\mathbf{NA}\cdot\mathbf{NQ}' = (\sin\theta_0 - n_x)(q - n_x) + (\cos\theta_0 - n_z)^2,$$

which after some simplification gives

$$\cos\theta = -\cot\zeta\cot(\zeta-\theta_f) + \cos\theta_0\csc\zeta\csc(\zeta-\theta_f) = \frac{-\cos\zeta\cos(\zeta-\theta_f) + \cos\theta_0}{\sin\zeta\sin(\zeta-\theta_f)}. \tag{B8}$$

[1] M. A. Nielsen and I. L. Chuang, *Quantum Computation and Quantum Information* (Cambridge University Press, Cambridge, England, 2000).
[2] D. Deutsch, A. Barenco, and A. Ekert, Proc. R. Soc. London, Ser. A **449**, 669 (1995).
[3] A. W. Knapp, *Lie Groups Beyond an Introduction*, Progress in Mathematics, 2nd ed. (Birkhauser, Boston, 2002), Vol. 140.
[4] S. Shi and H. Rabitz, J. Chem. Phys. **92**, 364 (1990).
[5] S. G. Schirmer, M. D. Girardeau, and J. V. Leahy, Phys. Rev. A **61**, 012101 (1999).
[6] Y. Maday and G. Turinici, J. Chem. Phys. **118**, 8191 (2003).
[7] N. Khaneja, R. Brockett, and S. J. Glaser, Phys. Rev. A **63**, 032308 (2001).
[8] Y. Ohtsuki, G. Turinici, and H. Rabitz, J. Chem. Phys. **120**, 5509 (2004).
[9] N. Khaneja, T. Reiss, C. Kehlet, T. Schulte-Herbrueggen, and S. J. Glaser, J. Magn. Reson. **172**, 296 (2005).
[10] S. Schirmer, J. Mod. Opt. **56**, 831 (2009).
[11] D. J. Siminovitch, Concepts Magn. Reson. **9**, 211 (1997).
[12] C. D. Hill, L. C. L. Hollenberg, A. G. Fowler, C. J. Wellard, A. D. Greentree, and H.-S. Goan, Phys. Rev. B **72**, 045350 (2005).
[13] J. Gorman, D. G. Hasko, and D. A. Williams, Phys. Rev. Lett. **95**, 090502 (2005).
[14] L. Euler, St. Petersburg Academy of the Sciences **2**, 43 (1862).
[15] M. Levitt and R. Freeman, J. Magn. Reson. (1969-1992) **33**, 473 (1979).
[16] M. Levitt, Prog. Nucl. Magn. Reson. Spectrosc. **18**, 61 (1986).
[17] H. K. Cummins and J. A. Jones, New J. Phys. **2**, 6 (2000).
[18] M. Testolin, Ph.D. thesis, University of Melbourne, 2008.
[19] S. G. Schirmer, A. Kolli, and D. K. L. Oi, Phys. Rev. A **69**, 050306(R) (2004).
[20] J. H. Cole, S. G. Schirmer, A. D. Greentree, C. J. Wellard, D. K. L. Oi, and L. C. L. Hollenberg, Phys. Rev. A **71**, 062312 (2005).
[21] J. H. Cole, A. D. Greentree, D. K. L. Oi, S. G. Schirmer, C. J.

Wellard, and L. C. L. Hollenberg, Phys. Rev. A **73**, 062333 (2006).
[22] S. G. Schirmer and D. K. L. Oi, Phys. Rev. A **80**, 022333 (2009).
[23] J. Zhang and K. B. Whaley, Phys. Rev. A **71**, 052317 (2005).
[24] K. C. Chatzisavvas, C. Daskaloyannis, and C. P. Panos, J. Quantum Comput. Comput. **4**, 93 (2003).
[25] K. C. Chatzisavvas, C. Daskaloyannis, and S. G. Schirmer, in *Computation in Modern Science and Engineering: Proceedings of the International Conference on Computational Methods in Science and Engineering*, edited by T. E. Simos and G. Maroulis, AIP Conf. Proc. No. 963 (AIP, New York, 2007) (Vol. 2B), p. 748.
[26] J. Zhang, J. Vala, S. Sastry, and K. B. Whaley, Phys. Rev. Lett. **93**, 020502 (2004).
[27] H. A. Sa Earp and J. K. Pachos, J. Math. Phys. **46**, 082108 (2005).
[28] V. Ramakrishna, K. Flores, H. Rabitz, and R. J. Ober, Phys. Rev. A **62**, 053409 (2000).
[29] F. Lowenthal, Can. J. Math. **24**, 713 (1972).
[30] D. D'Alessandro, Automatica **40**, 1997 (2004).
[31] S. Schirmer and P. Pemberton-Ross, Phys. Rev. A **80**, 030301(R) (2009).
[32] P. E. Crouch and Silva Leite, Syst. Control Lett. **2**, 341 (1983).
[33] F. Silva Leite, Rocky Mt. J. Math. **21**, 879 (1991).
[34] The decomposition of individual gates is not always unique. In some (rare) special cases the algorithm may produce a decomposition that can be simplified further. If we choose the orthogonal axes $\hat{\mathbf{h}}=\hat{\mathbf{z}}=(0,0,1)^T$ and $\hat{\mathbf{g}}=\hat{\mathbf{x}}=(1,0,0)^T$, for example, then Algorithm 1 returns $\boldsymbol{\epsilon}=(\frac{3}{2}\pi,\pi,\frac{3}{2}\pi)$ for the swap gate σ_x, whose $\mathrm{SO}(3)$ representation is $R_X=\mathrm{diag}(1,-1,-1)$, which corresponds to the decomposition $R_{\hat{\mathbf{h}}}(\frac{3}{2}\pi)R_{\hat{\mathbf{g}}}(\pi)R_{\hat{\mathbf{h}}}(\frac{3}{2}\pi)$ and can be simplified to $R_{\hat{\mathbf{g}}}(\pi)$ as $R_{\hat{\mathbf{z}}}(a)R_{\hat{\mathbf{x}}}(\pi)R_{\hat{\mathbf{z}}}(a)=R_{\hat{\mathbf{x}}}(\pi)$ for any $a\in\mathbb{R}$.